Self–Assembly versus Directed Assembly of Nanoparticles via Pulsed Laser Induced Dewetting of Patterned Metal Films

5 AUTHORS, INCLUDING:

Jason D Fowlkes
Oak Ridge National Laboratory
136 PUBLICATIONS **2,232** CITATIONS

Lou Kondic
New Jersey Institute of Technology
189 PUBLICATIONS **1,648** CITATIONS

Javier Alberto Diez
National University of Central Buenos Aires
92 PUBLICATIONS **1,000** CITATIONS

Self-Assembly versus Directed Assembly of Nanoparticles via Pulsed Laser Induced Dewetting of Patterned Metal Films

Jason D. Fowlkes,*,[†] Lou Kondic,[‡] Javier Diez,[§] Yueying Wu,[‖] and Philip D. Rack[†,‖]

[†]Center for Nanophase Materials Sciences, Oak Ridge National Laboratory, Oak Ridge, Tennessee 37831-6493

[‡]Department of Mathematical Sciences, Center for Applied Mathematics and Statistics, New Jersey Institute of Technology, Newark, New Jersey 07102

[§]Instituto de Fisica Arroyo Seco, Facultad de Ciencias Exactas, Universidad Nacional del Centro de la Provincia de Buenos Aires Pinto 399, 7000, Tandil, Argentina

[‖]Materials Science and Engineering Department, The University of Tennessee, Knoxville, Tennessee 37996-2200

S *Supporting Information*

ABSTRACT: A nanoscale, synthetic perturbation was all that was required to nudge a natural, self-assembly process toward significantly higher order. Metallic thin film strips were transformed into nanoparticle arrays by nanosecond, liquid-phase dewetting. Arrays formed according to an evolving Rayleigh—Plateau instability, yet nanoparticle diameter and pitch were poorly controlled. However, by patterning a nanoscale sinusoid onto the original strip edge, a precise nanoparticle diameter and pitch emerged superseding the naturally evolving Rayleigh—Plateau instability.

KEYWORDS: Directed assembly, Rayleigh—Plateau, pulsed laser melting, nanoscale lithography, thin film dewetting
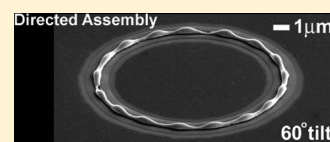
Materials self-assembly predicated on easily defined initial conditions constitutes a groundbreaking demonstration of advanced materials synthesis. Nature provides the preeminent model of efficiency, parallel action, and integration toward achieving complex, functional systems. The conversion of a simple input yielding a complex output is critical for natural systems. Taking a cue from natural systems, we have demonstrated a materials assembly method, based on nanofabrication, where a very simple input geometry (*a simple thin film strip*) was designed to produce a more complex output (*a precise, linear array of nanoparticles*) by making use of a naturally occurring instability, present in cylindrical fluid rivulets. Self-assembly was activated by pulsed laser induced dewetting (PLiD).[1−8] Capillary forces initially drive the assembly through the large surface-to-volume ratio present in the thin film strip.[7] Concurrently, the solid—liquid forces between the substrate and liquid rivulet stabilize the nanoparticle assembly.[9] *Moving one step further, an extremely sensitive switch was devised to direct the natural self-assembly process by designing an initial condition.* A nanoscale, synthetic sinusoidal perturbation imposed on the thin film strip edge led to an outstanding improvement in the precision and accuracy of the nanoparticle pitch and size relative to the freely propagating, natural fluid instability. The switch sensitivity proved ideal for directing assembly—slight, nanoscale changes in the initial sinusoid amplitude (∼20 nm) led to a drastic improvement in assembly fidelity.

Nanofabrication makes it possible to deposit materials systems that are far from equilibrium. Materials can be synthesized by physical vapor deposition and nanoscale lithography that have external geometries unachievable at thermal equilibrium. Such nonequilibrium materials rapidly reorganize into structures with fascinating spatial/morphological properties when subjected to brief yet high energy input.

Pulsed laser melting offers a unique opportunity to dictate materials assembly where rapid heating and cooling rates (10^{10} K/s) and nanosecond melt lifetimes are achievable. *Liquid lifetimes either less than, or on the order of, the self-assembly time scale afford a unique opportunity to actively observe, engage, and control the assembly process.* The SPEL (self-perfection by liquefaction) method provides a notable demonstration of the power of nanosecond, pulsed laser melting to refine nanoscale features and elements.[10] *Here, nanosecond PLiD was used to transform thin film metal strips with and without sinusoidal perturbations imposed on the boundaries into linear nanoparticle arrays by directing the natural evolution of a Rayleigh—Plateau (RP) liquid instability*[11−16] *modified by the solid substrate—liquid rivulet interaction.* The RP instability has been used previously to create nanostructures where both ion[17] and photon beams[8,18] were used to organize patterned metals. Xia et al. used periodicity engineering in the substrate to affect RP assembly.[8] In this work, we both engage and direct the RP instability by simply imposing a nanoscale perturbation on the initial geometry of the thin film strip. Linear arrays of ordered, metallic nanoparticles are desirable for a number of nanotechnology applications including plasmon resonance waves,[19] nanomagnetism,[20,21] magnetic recording via plasmon antennas[22] and storage.[23]

Mechanistically, the patterned metal (Ni) strips are laser irradiated above their melt threshold, inducing the liquid phase

retraction of the flat strips to a rivulet shape during the intermediate stages of the process; a static cylindrical fluid jet results, truncated along the jet axis by the substrate. On the rivulet, a range of varicose oscillations become unstable leading to the formation of droplets as the rivulet breaks up. *Without synthetic perturbations, the varicose modes*[8,18] *of wavelengths close to the most unstable one, characterized by the fastest growth rate for the rivulet geometry, ultimately sets the natural variation, i.e., dispersion, of the nanoparticle pitch and size.* In contrast, the precision achieved in nanoparticle size and spacing, accomplished by imposing synthetic perturbations, overwhelmingly exceeds that attainable by the natural RP-like destabilization process.

While there are differences in the driving forces that participate in the destabilization of a substrate-supported liquid rivulet (viscosity, capillary, and liquid–solid interaction) compared with a free-standing, Rayleigh–Plateau jet (inertial and capillary forces) as summarized by Diez et al.,[9] we refer to the destabilization of a substrate supported rivulet as a modified Rayleigh–Plateau instability, since we have shown that the results of the two instability mechanisms are comparable for the nanoscale liquid metals studied here.[18,24] Notably, liquid phase self-assembly via the spinodal, or thin film instability,[1–3,6,24–26] has also been explored for a host of metallic materials where a similar disperse nanoparticle size and spacing distribution results as a consequence of the hydrodynamic evolution of the underlying instability. In addition, solid-state dewetting driven by surface diffusion[27] also leads to nanoparticle formation.[28–30]

We report the following: (1) Without synthetic perturbations, the rivulet destabilization into droplets can be understood based on the modified RP instability mechanism, leading to the formation of dispersed nanoparticles. (2) Synthetic nanoscale varicose perturbations, characterized by a length-scale larger than a critical wavelength, lead to a drastic reduction in particle dispersion (as measured by the particle size and pitch of the final, organized structure). (3) Linear stability analysis (LSA) of the modified RP model correctly predicts the initial stages of the instability development as well as the critical wavelength required for synthetic perturbations to yield ordered structures. (4) Nonlinear time-dependent simulations of hydrodynamic evolution reproduce detailed nanoscale spatial and temporal features observed during both liquid phase retraction and instability growth.

Brief Methods: Rivulet Formation Starting from Thin, Nanoscale Metallic Films. The objective of our methodology is to precisely organize an array of nanoparticles originating from the dewetting of a liquid rivulet. This, however, requires the creation of the semicylindrical rivulet which is difficult by standard nanolithography (**S1** in Supporting Information). Instead, a very thin film strip was deposited, which was designed to retract upon melting into the desired nanoscale rivulet geometry. Nanolithography (see Methods) along with physical vapor deposition was used to define metallic (nickel, Ni) thin film strips with both straight (Figure 1a) and sinusoidal edges (shown later). The cross-sectional area of the thin film strip was designed to contract into a truncated liquid rivulet of radius (R_o) according to the following area balance

$$h \times w = \theta_o R_o^2 - R_o^2 \sin \theta_o \cos \theta_o \qquad (1)$$

where θ_o is the equilibrium contact angle between the liquid Ni rivulet and silicon substrate. The angle θ_o is dictated by the Young–Laplace equation. The rivulet morphology (Figure 1b)

results from the conversion of the thin film strip (Figure 1a) into a liquid by nanosecond PLiD. The straight edged strips (Figure 1a) were designed to self-assemble as governed by the modified RP instability.

The brief liquid lifetime per pulse (7.5–14.9 ns) produced during PLiD was on the same order of magnitude as both the fluid transport[5,7] and modified RP instability time scales[12,14,15,18,24] which govern the rivulet self-assembly process and nanoparticle breakup, respectively. This convergence of time scales, coupled with the rapid heating and cooling rates, made it possible to capture and visualize the temporal dynamics of the morphology evolution by repetitively pulsing and electron imaging (see **S2** in the Supporting Information for an example of a typical time–temperature plot).[1]

Nanoparticle Self-Assembly, Derived from the Evolution of the Rivulet Instability. Destabilization of the rivulet morphology into a linear nanoparticle array begins with the growth of surface perturbation modes on the rivulet surface as shown in Figure 1c. The fastest growing modes ultimately out-pace slower ones, breaking up the rivulet into droplets which resolidify. The resulting nanoparticle arrays exhibit a significant dispersion in nanoparticle radius and pitch.[8,18] Panels d and e of Figure 1 show the growth rate (ω) versus wavelength (λ) curve, i.e., dispersion curve, estimated from both the standard RP theory of a fluid jet (blue solid line) as well as from the LSA based on the modified RP mechanism (blue dashed lines) for a Ni rivulet on a Si substrate with a radius of (Figure 1d) 130 ± 18 nm and (Figure 1e) 165 ± 9 nm. Arriving at a desired nanoparticle size and pitch requires a detailed knowledge of the RP instability which dictates the assembly time and length scale.[8,18,31] The modified RP mechanism gives a better prediction of the dispersion curve since substrate effects are considered. This can be seen in panels d and e of Figure 1 by examining the position of dispersion curve maximum relative to the superimposed histogram of final nanoparticle pitch. In order to understand the origins of these instability mechanisms, we briefly review both theories.

The RP model for a fluid jet predicts that varicose modes, characterized by the wavelength exceeding the critical one (λ_c), evolve as a result of the interaction between transverse and transaxial pressure gradients in the fluid. Ignoring interaction with the substrate, one may consider that the pressure gradients arise in the liquid rivulet due to the presence of small oscillations on the rivulet surface. The growth rate of a perturbation of wavelength ($\lambda = 2\pi/k$), according to RP model is

$$\omega^2 = \frac{\gamma}{\rho R_o^3} k R_o \frac{I_1(k R_o)}{I_o(k R_o)} \left(1 - k^2 R_o^2\right) \qquad (2)$$

where γ is the liquid–vapor surface tension, ρ is the liquid density, k is the wavenumber, and $I_n(k R_o)$ are nth order hyperbolic Bessel functions.[11,13,15] This expression predicts that only the varicose surface modes of $\lambda_c > 2\pi R_o$ are unstable and therefore yield droplets. The fastest growing mode satisfies $\lambda_m \sim 9.02 R_o$.

The modified RP mechanism is derived by applying the lubrication approximation to model the evolution of a liquid rivulet *supported on a solid substrate*. The approach implemented here is based on lubrication approximation,[9] which yields the following equation

$$3\mu \frac{\partial h}{\partial t} + \gamma \nabla(h^3 \nabla \nabla^2 h) + \nabla[h^3 \nabla \Pi(h)] = 0 \qquad (3)$$
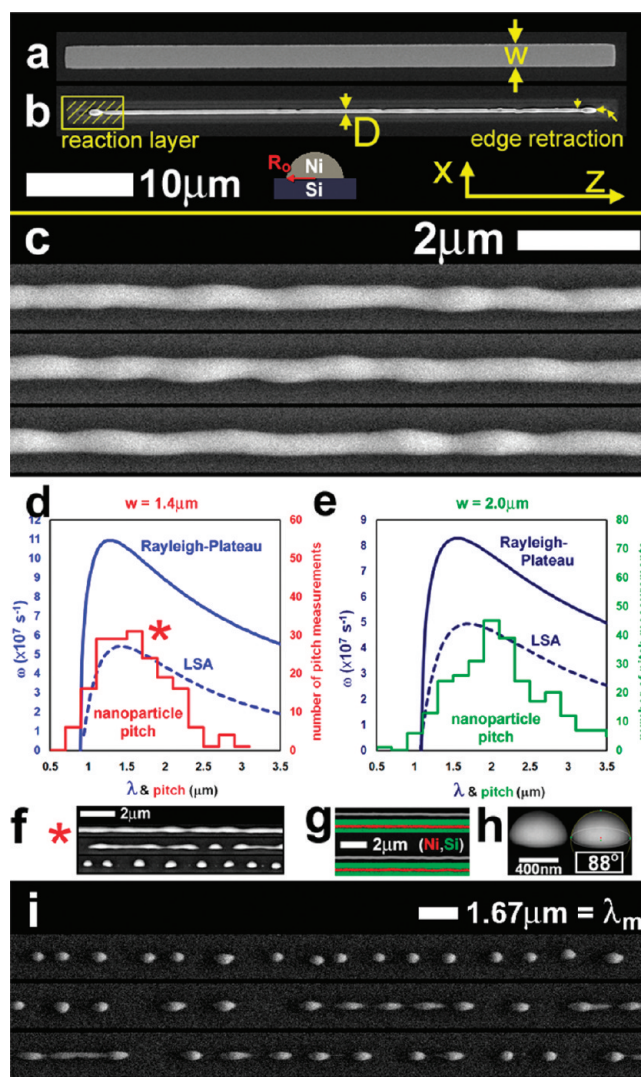
Figure 1. Self-assembly in the liquid phase by the modified Rayleigh−Plateau instability. The PLiD self-assembly method starts by converting a thin film strip into a rivulet. (a) A scanning electron microscopy (SEM) image of a Ni thin film strip following electron beam lithography and metallization. The image was acquired normal to the Si substrate surface. The thin film strip dimensions were height (h) = 23 ± 1.2 nm, width (w) = 2.05 μm ± 18 nm, and a length of 50 μm. (b) Strips rapidly transform, by fluid retraction, into a rivulet upon pulsed laser melting. A liquid rivulet with a radius (R_o) of 165 ± 9 nm results following five KrF 248 nm laser pulses and an energy density of 420 mJ/cm^2 (liquid lifetime 5 × 14.9 ns = 74 ns). An ultrathin reaction layer forms simultaneously during retraction which is presumably a very thin silicide (Ni$_x$Si$_y$). This layer conveniently imprints the original strip dimension. Out-of-plane capillary forces drive the indicated (yellow arrows) edge and vertex retraction.[7,32] (c) A modified Rayleigh−Plateau instability induces surface perturbations once the rivulet forms. In this case, the original thin film strip width (w) was 1.4 μm ± 18 nm. A rivulet of R_o = 130 ± 18 nm was formed following liquid phase retraction during 10 pulses of E_d = 380 mJ/cm^2. (d, e) Rivulet breakup occurs at varicose troughs. As a result, the final nanoparticle spacing distribution mirrors the dispersion curve (ω vs λ) which dictated its formation. Linear stability analysis (LSA) based on the modified RP instability mechanism predicts the growth rate of unstable varicose perturbations as a function of their wavelength (i.e., the dispersion curve) for the (d) 130 nm rivulet and (e) 165 nm rivulet as shown by the blue, hatched lines. The original thin film strip dimensions were (d) w = 1.4 μm ± 18 nm, h = 23 ± 1.2 nm and (e) w = 2.05 μm ± 18 nm, h = 23 ±1.2 nm. Both thin film strips were 50 μm long. The RP prediction for a free jet (without the effects of the substrate) is also shown (solid, blue lines). Histogram plots of the nearest-neighbor, nanoparticle spacing (R_o = 130 nm, green histogram and R_o = 165 nm, red histogram plot) reveal a strong correlation between the LSA predicted perturbation growth rate (ω) and final nanoparticle pitch. The pitch bin width for both histogram plots was 200 nm. (f) Tilted SEM images (∼45°) of the three stages of self-assembly for the R_o = 130 nm rivulet; top-to-bottom, perturbations on the rivulet, partial rivulet breakup, and nanoparticle chain formation (the SEM image indicated by (*) is a representative image from which the pitch histogram in (d) was derived). The original thin film strip dimensions were w = 1.4 μm ± 18 nm, h = 23 ± 1.2nm. The thin film strip was 50 μm long. (g) Complementary secondary electron and energy dispersive spectroscopy (EDS) maps confirming the rivulets are nickel (see Methods) for the same thin film strip dimension as shown in (f). (h) The equilibrium contact angle θ_o between the final Ni nanoparticle and Si substrate surface was determined to be 88 ± 5° by image analysis of tilted SEM images following 20 pulses using E_d = 380 mJ/cm^2. The SEM image was acquired at a stage tilt of 60°. (i) The variation in the dewetted nanoparticle pitch mirrors the dispersion in the underlying modified, RP instability. The scale bars have deliberately been set to equal the fastest growing mode as predicted by LSA—the nanoparticle pitch closely reflects this value. The original thin film strip was 1.4 μm ± 18 nm wide, 23 ± 1.2 nm tall, and 50 μm long.

where $h(x,y,t)$ is the Ni liquid thickness, μ is the viscosity of liquid Ni, and $\Pi(h)$ represents the disjoining pressure which accounts for the interaction between rivulet and substrate. Linear stability analysis applied to eq 3 gives predictions for the evolution of small perturbations of the liquid rivulet surface; for simplicity we refer to the results of this model in the limit of small disturbances as "LSA". LSA predicts that the rivulet is stabilized by the presence of a substrate, where the extent of the stabilization is a function *of* the wetting angle of the fluid on the substrate.[9]

On the basis of the modified RP mechanism, one expects the perturbations characterized by the growth rate close to the maximum (λ_m) to be dominant. Indeed, the final nanoparticle pitch is close to λ_m. This can be clearly gleaned from our experimental results in Figure 1d showing the overlap of the nanoparticle pitch histogram and the LSA prediction. The resulting nanoparticle diameter is likewise set by the wavelength as well as by the initial rivulet radius.

Panels d and e of Figure 1 demonstrate several characteristics of the LSA results (dashed lines): (1) negative growth rates for $\lambda < 900$ nm ($R_o = 130$ nm) and $\lambda < 1100$ nm ($R_o = 165$ nm) indicate stable varicose modes which ultimately decay on the rivulet surface favoring a smooth rivulet, i.e., no nanoparticle formation; (2) a maximum exists in the growth rate curve indicating a maximum growth rate of $\omega = 5.2 \times 10^7\,\mathrm{s}^{-1}$ at $\lambda_m = 1.45\,\mu$m ($R_o = 130$ nm) and $\omega = 5 \times 10^7\,\mathrm{s}^{-1}$ at $\lambda_m = 1.67\,\mu$m ($R_o = 165$ nm); (3) the full width at half-maximum (fwhm) of the curves is disperse since $\Delta\lambda \sim 1\,\mu$m. Importantly, ω specifies approximately the time scale at which the formation of nanoparticles is expected ($t_{scale} \sim 1/\omega \sim 20$ ns), which is on the same order of magnitude as in experiments. *The fact that there is a wide range of wavelengths characterized by similar growth rates yields a significant variation in nanoparticle pitch (and size) for the self-assembly process.*

The statistical distribution of nearest-neighbor nanoparticle pitch was strongly correlated with the dispersion curve indicating that the modified Rayleigh−Plateau instability ultimately governs the PLiD self-assembly process. For example, the nanoparticle pitch histogram (*red curve, right ordinate*) shown in Figure 1d for the $R_o = 130$ nm case overlaps well the LSA dispersion curve (left ordinate). This suggests close correlation of mode wavelength and nanoparticle pitch. In addition, the temporal evolution of perturbations prior to rivulet breakup was estimated from experiments by calculating the fast Fourier transform (FFT) of scanning electron microscopy (SEM) images (**S3**, Supporting Information) of rivulets. The FFT was found to provide an estimate of the amplitude distribution on the rivulet surface and could be directly compared to the dispersion curve. Remarkably, results indicated that (1) the final nanoparticle pitch is determined already at very early times, i.e., while perturbation amplitudes are of the order of 1−10 nm, (2) the experimental data are slightly shifted to longer wavelengths relative to the RP prediction which is consistent with the stabilizing influence of the substrate (compare the green and two blue curves in Figure 1e). Thus, the LSA estimate of dispersion dictated by the modified RP instability is found to accurately predict the dispersion of varicose modes observed experimentally.

Directed Nanoparticle Assembly: Controlling the Instability. Varicose perturbations characterized by a variety of wavelengths and amplitudes were lithographically patterned into the nickel thin film strips in order to explore the potential of directed-assembly to yield a very precise nanoparticle size and pitch. We refer to these modes as synthetic, in contrast to the naturally
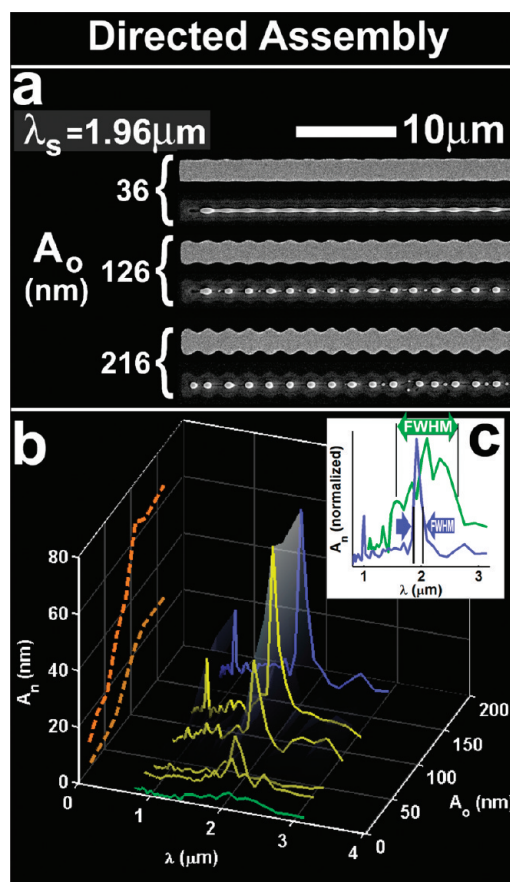
Figure 2. The transition from self-assembly to directed assembly. The directed assembly of linear nanoparticle arrays was accomplished by prescribing a single synthetic varicose perturbation on the initial thin film strip. (a) Varicose prescription effectively provides a "head start" for amplitude evolution for an unstable mode—larger amplitudes lead to a more rapid formation of nanoparticles. For example, the unstable mode shown ($\lambda = 1.96\,\mu$m) is still in the evolution phase for a synthetic perturbation of amplitude $A_o = 36$ nm while the equilibrium nanoparticle morphology has formed for the case of $A_o = 216$ nm. The experiments were conducted using a constant photon dose of five pulses at 420 mJ/cm². The average thin film strip width was $2.05\,\mu$m $\pm$ 18 nm and the thickness was 23 ± 1.2 nm. (b) Fast Fourier transforms (FFT) reveal the change from self-assembly to directed assembly with increasing initial amplitude. FFT's calculated at $A_o = 0$, 36, 44, 96, 126, and 196 nm reveal the emergence of a discrete peak at the synthetic wavelength ($\sim 2\,\mu$m) with increasing A_o. A less intense, satellite peak emerges at $\sim 1\,\mu$m and is predicted by nonlinear hydrodynamic simulations (see Figure 5a later). For clarity, the evolution of the Fourier components (A_n) of the ~ 1 and 2 μm modes as a function of initial varicose amplitude has been projected onto the $\lambda = 0\,\mu$m plane in the figure as orange, hatched curves. (c) The inset shows the Fourier spectra of the $A_o = 0$ nm (self-assembly) and $A_o = 216$ nm (directed assembly) cases. The spectra have been normalized in order to highlight (1) the narrow and discrete nature of the synthetic Fourier mode for the directed assembly case as well as (2) the similarity of the Fourier spectra, for the $A_o = 0$ nm case, to the curve predicted by LSA of the modified RP model (revisit Figure 1e), which is not surprising since the modes characterized by small growth rates lead to only a small contribution to the FFT spectra.

evolving modes which were shown above. Figure 2a demonstrates the as-synthesized nickel strips with a synthetic varicose perturbation for an average strip width of 2 μm and $\lambda = 1.96\,\mu$m

(*approximately the fastest growing mode as predicted by LSA, see* Figure 1e) and various amplitudes. Below each strip we show the resultant morphology following PLiD using a fluence of 420 mJ/cm² (five pulses) which revealed striking results: (1) the synthetic mode is maintained with high fidelity, through the liquid retraction phase of assembly, (2) the larger amplitude perturbations result in nanoparticles aligned at the peaks of the original synthetic perturbations, and (3) rivulet pinch-off (as well as satellite droplets) occurs at the perturbation troughs.

FFTs derived from the final dewetted morphologies were used to ascertain the effect of the initial perturbation amplitude (Figure 2b). The zero initial amplitude experiments (green FFT) were effectively straight thin film strips. In this case, nanoparticle formation is ultimately governed by the LSA predicted instability as demonstrated previously. *By imposing a single wavelength, we effectively silence the thermally generated perturbations since the prescribed mode has a significant competitive advantage in terms of its initial amplitude.* The synthetic varicose perturbation effectively provides a "head start" for the amplitude evolution of an unstable mode—larger amplitudes lead to a more rapid formation of nanoparticles. Interestingly, this process hinges on the selection of an *unstable mode*. For example, the unstable 1.96 μm mode (Figure 2b) both intensifies and sharpens with increasing amplitude as a high fidelity array of nanoparticles emerges. *We have found that the FFT spectra closely mimic nanoparticle pitch histograms, with the fwhm of the distribution reflecting the variation in nanoparticle pitch.* Figure 2c shows clearly the narrowing of the pitch dispersion, i.e., a smaller fwhm, for *PLiD directed assembly* (A_o = 216 nm, blue line) compared with the *PLiD self-assembly* results (A_o = 0 nm, green line). These Fourier spectra have been normalized to compare the fwhm of the respective curves. Remarkably, unstable synthetic perturbations as small as $A_o \sim$ 20 nm yielded nanoparticles with a pitch equal to the unstable synthetic wavelength (**S4**, Supporting Information).

The wavelength dependence of the synthetic perturbation evolution was studied by patterning thin film strips with *unstable* wavelengths (1.352 and 1.96 μm). With the average strip width kept constant, the results could be compared with the results for unpatterned strips previously shown in Figure 1e. In addition, a *stable* wavelength (λ = 800 nm) exhibiting a negative growth rate was also explored. *Synthetic perturbations of stable wavelengths were found not to grow, even if prescribed with an amplitude constituting up to 20% of the thin film strip width.* Figure 3 summarizes the results for these experiments. Figure 3a shows SEM images of three distinct varicose perturbations where the amplitude (108 nm) and fluence were fixed. This produces a nearly constant liquid lifetime across the experimental set. As expected, the faster growing wavelength of the subset (*1.96 μm as predicted by LSA*, Figure 1e) is transformed into nanoparticles with a pitch reflecting the prescribed wavelength, whereas the relatively slower growing mode (1.352 μm) has only begun to break up. Remarkably, the stable varicose perturbation (800 nm) has decayed in amplitude favoring the transformation to a smooth rivulet. This result is consistent with the LSA results (Figure 1e), which suggest negative growth rates below λ < 1.1 μm.

Figure 3b shows an SEM image collage of 15 laser irradiated thin film strips (amplitude increasing from top to bottom in the figure) for the λ = 1.352 μm synthetic perturbation. Nanoparticles formed faster for larger initial amplitudes with a pitch reflecting the synthetic wavelength. Nanoparticles were less developed with decreasing amplitude. Oscillating, fragmented rivulets were observed for the smallest amplitudes. Figure 3c is a
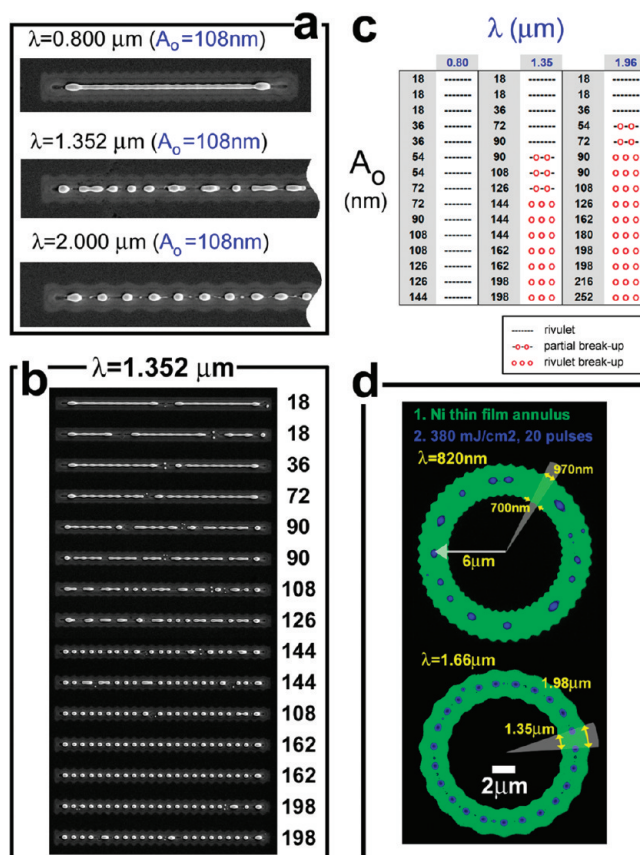
Figure 3. Directed assembly by instability engagement using a nanoscale, synthetic perturbation. (a) Synthetic modes were found to be either stable (λ = 0.8 μm) or unstable (λ = 1.352 and 2 μm) as predicted by LSA. (b) Nanoparticle formation, i.e., rivulet breakup, was accelerated with increasing initial synthetic amplitude. The amplitude, in nanometers, imposed at the edge of each Ni thin film strip is shown at the right of each SEM image. The same photon dose was used as in (a). (c) The table shows a summary of the final Ni morphology as a function of initial synthetic wavelength and amplitude. The photon dose is the same as in (b). The stable mode (λ = 0.8 μm) decays back to the rivulet, without breakup, regardless of the magnitude of the initial amplitude. Among the unstable modes, the 1.96 μm mode forms nanoparticles more rapidly, for smaller magnitudes of A_o, when compared with the 1.35 μm mode since the growth rate for the 1.96 μm mode is greater (see the LSA curve in Figure 1e). The strip geometries and photon irradiation conditions for the data shown in (a−c) were five laser pulses, E_d = 420 mJ/cm², w = 2.05 μm ± 18 nm and h = 23 ± 1.2 nm). (d) The natural instability begins evolving in the thin film strip, patterned with the 820 nm stable mode. A fluence of 380 mJ/cm² and 20 laser pulses was applied to the Ni thin film annulus patterned with the 820 nm stable varicose mode (falsely colored as green in the SEM overlay image collage). The thin film annulus was 26 ± 1.2 nm thick and 2.36 μm ± 18 nm wide. The 820 nm synthetic perturbation decayed during the 20 laser pulses followed by rivulet breakup leading to a particle spacing consistent with the fastest growing unstable mode predicted by the modified Rayleigh−Plateau instability (blue, falsely colored SEM image) (**S5**, Supporting Information). In contrast, the unstable 1.66 μm mode yields a nanoparticle pitch consistent with the imposed synthetic perturbation for the same photon dose.

table summarizing the morphology for various combinations of wavelength and amplitude. *Consistent with our expectations, the table demonstrates that unstable wavelengths with larger growth rates require smaller synthetic amplitudes for discrete mode selection.*
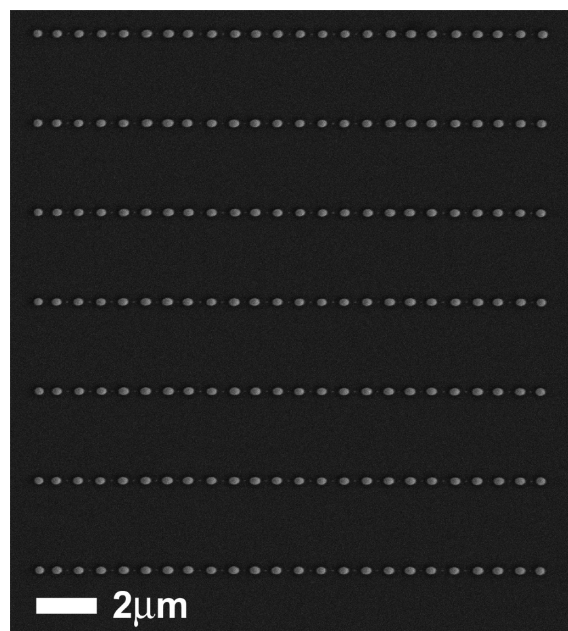
Figure 4. Directed assembly leads to the formation of high fidelity nanoparticle arrays. The nanoparticle arrays were derived from seven thin film strips originally oriented along the lateral dimension of the figure. PLiD was initiated using an energy density of 400 mJ/cm^2 and five laser pulses. The starting thin film strip contained a sinusoidal synthetic perturbation with a 720 nm wavelength. The initial amplitude of the perturbation in the thin film strip was 72 ± 24 nm. The thin film strip height was 23 ± 1.2 nm and the average width of the strip was 408 ± 24 nm. The synthetic perturbation translated into an unstable varicose perturbation of the same wavelength in the intermediate rivulet. As a result, the final nanoparticle pitch was 720 ± 48 nm and the nanoparticle radius was 142 ± 24 nm.

The nanoparticle formation time scale was consistent with the predictions of the LSA.

Longer liquid lifetimes (additional laser pulses) were required to observe the self-assembly for the *stable* varicose perturbation. Figure 3d shows a thin film annulus with an average synthetic wavelength of 820 nm (green feature) and the resultant nanoparticles (blue) overlaid on the original image. Annular films are convenient because they mitigate edge retraction effects (Figure 1b) observed during the dewetting of strips.[24] The 820 nm mode is stable and does not reproduce the patterned wavelength. A dispersive nanoparticle size and pitch resulted which was consistent with the evolution of the natural, disperse instability. The synthetic perturbation first decays leading to an apparently smooth, annular rivulet. This rivulet evolves into a nanoparticle array, as predicted by LSA, and not by the synthetic mode. This scenario is supported by a complementary control experiment (**S5**, Supporting Information) which shows that the same distribution in nanoparticle pitch and size is obtained, whether or not the starting thin film annulus was smooth or patterned with a stable, synthetic 820 nm mode. Conversely, the second annulus shown in Figure 3d was synthetically perturbed by an *unstable* varicose wavelength (1.66 μm). A remarkably precise nanoparticle size and pitch results following dewetting, which is consistent with the prescribed 1.66 μm mode. Nanoparticle arrays are shown in Figure 4 which exhibits the remarkable accuracy and precision in nanoparticle pitch/radius that results when PLiD directed assembly is carried out to completion.
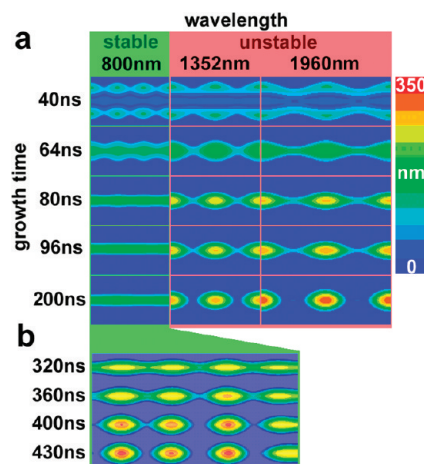
Figure 5. Directed assembly as predicted by nonlinear hydrodynamic simulations. Nonlinear hydrodynamic simulations of 2 μm wide Ni thin film strips ($h = 23$ nm) with an initial synthetic amplitude of $A_o = 108$ nm. The simulations were performed to emulate the experimental results shown in Figure 3a. (a) The synthetic perturbation characterized by $\lambda = 800$ nm decays and leads to a smooth and uniform rivulet on the time scale spanning 200 ns. In contrast, the perturbations characterized by $\lambda = 1352$ and 1960 nm lead to the formation of nanoparticles during this time scale as seen in experiments. (b) For longer times, the Ni thin film strip perturbed by the 800 nm edge mode breaks up into nanoparticles whose particle separation is much larger than the initially imposed wavelength. Similarly to the experiment for the $\lambda = 820$ nm case (strip width of 2.4 μm) shown in Figure 3d, a nanoparticle spacing consistent with the fastest growing mode sets the final nanoparticle pitch.

To complement the experimental observations and predictions from LSA, fully nonlinear three-dimensional hydrodynamic simulations were performed (**S6**, Supporting Information). For brevity, we only show the consistency of the results with the experiments, as well as some new insights reached. Figure 5 shows the temporal evolution of the experimentally explored wavelengths of 800, 1352, and 1960 nm for the synthetic perturbation amplitude of 108 nm. For $\lambda = 1352$ and 1960 nm, the distance between the dewetted nanoparticles corresponds to the prescribed wavelength as predicted by LSA, in agreement with the experiments (Figure 3a). Also, the nanoparticle formation time scale is consistent, although slightly longer, than the time observed experimentally (Figure 3a). We note that the simulations capture even some subtle details of the experiments, such as the formation of satellite nanoparticles visible in the simulations for $l = 1960$ nm and in the experiments in Figures 2 and 4. While we find it curious that these features appear regularly only for larger wavelengths, we defer their careful analysis to future work. In contrast, the short wavelength perturbation ($\lambda = 800$ nm) did not break up but rather formed a uniform rivulet on the time scale considered in Figure 5a. However, at longer times, nanoparticles emerged with a pitch much larger than the prescribed 800 nm perturbation. Additional imposed random perturbations characterized by a range of wavelengths and small random amplitudes prevailed and the resulting pitch was consistent with the linearly unstable wavelengths (Figure 5b).

Self-assembly and directed assembly of metallic nanoparticle arrays were accomplished by synthesizing nickel thin film structures far from equilibrium and initiating their assembly via pulsed laser melting. The modified Rayleigh−Plateau instability mechanism, including the effect of fluid−solid interaction, was

found to faithfully describe the main features of the instability process, including the relevant time scales, where a fluid rivulet destabilized into an array of nanoparticles. Yet, the spacing between nanoparticles and the distribution of nanoparticle radii is unacceptably disperse for many practical applications. This variation in pitch and size resulted from the presence of a multitude of unstable modes which randomly evolve on the rivulet surface. We engaged and directed the natural assembly process by prescribing "synthetic", unstable modes in the starting thin film structure. The synthetic mode in the strip (a sinusoid located along the strip edges) translated into an unstable varicose oscillation on the rivulet. Rivulet breakup ensued. A precise, controlled nanoparticle size and pitch emerged thereby superseding the otherwise naturally evolving modes predicted by the modified RP instability. Linear stability analysis of the modified RP model predicted experimentally observed nanoparticle distributions for the self-assembly process and suggested the properties of synthetic perturbations leading to desired results. Nonlinear hydrodynamic simulations reproduced the nanoscale spatial/temporal features observed in the assembly process, captured in the resolidified nanoparticle morphologies. Simulation predictions were accurate both for the naturally evolving self-assembly process as well as for the directed assembly method used to tailor the final nanoparticle size and pitch. While unstable modes could be synthetically selected; synthetic, stable modes decayed and natural mode selection by the RP instability ensued.

Methods. *Electron Beam Lithography.* Nickel thin film strips of micro- and nanoscale dimensions were defined on Si wafer substrates using electron beam lithography (EBL) followed by direct current (dc) magnetron sputtering. Focused electron beam exposure at 10 keV and 150 pA was performed using an FEI Nova 600 microscope combined with Raith ELPHY Quantum pattern generation software. A poly(methyl methacrylate) (PMMA)-based, positive tone electron resist 495-A4 provided by Shipley was exposed for pattern definition. The PMMA resist was spin-coated on a Si wafer chip ~ 1 cm^2 in area at 4000 rpm for 60 s. Spin coating was followed by a 2 min, 180 °C hot plate bake. An exposure dose of 240 μC cm^{-2} was required to completely expose the electron resist in order to produce well-defined and nanoscale thin film strip edges capable of supporting lateral sinusoid oscillations with an amplitude (A_o) of 20 nm or greater. Pattern exposure was accomplished using the Raith software package coupled with an external electron beam blanker attached to the FEI Nova microscope. Feature dimensions for scanning electron exposure were contracted by 15% in order for design dimensions to be precisely replicated in the PMMA resist owing to the proximity effect where the superfluous exposure of resist occurs beyond the extent of the intended and scanned region. Each individual feature was exposed using an electron probe step size of 16 nm and a dwell time per exposure pixel of 4.1 μs producing an electron probe exposure velocity of 3.9 mm s^{-1}. An exposure write-field size of 100 μm $\times$ 100 μm was used to expose a linear array of thin film strip features spaced apart uniformly on a square grid array, most often but not restricted to a 5 μm pitch. The write-field size was geometrically calibrated prior to exposure using a microfabricated checkerboard array of 10 μm squares to accurately pattern the designed features (a so-called Chessy pattern Si chip provided by Raith). The 495-A4 resist development was carried out in a 1:3 methyl isobutyl ketone (MIBK)/isopropyl alcohol (IPA) solution for 100 s followed by an IPA rinse that physically revealed the exposed patterns in the resist. The thin film strips were exposed completely down to the underlying silicon substrate, surrounded by unexposed resist. An 8 s exposure of the Si chip to an oxygen plasma generated in a reactive ion etcher (100 W capacitively coupled plasma, 10 cm^3 min^{-1} O$_2$ flow and a pressure setting of 150 mTorr) was implemented in order to remove any ancillary residual resist from the exposed regions. Metal was then deposited in the exposed pattern.

dc Sputter Deposition. An AJA International 200 dc magnetron sputter deposition system was used to deposit the Ni thin film strips. Sputter deposition was conducted using the constant power mode at 30 W under a constant chamber pressure of 3 mTorr Ar. A static pressure was maintained with a gas flow rate of 25 cm^3 min^{-1}. The resulting sputter rate of Ni was 5.8 nm min^{-1} for a target-to-substrate distance of $\sim$5 cm. A wet, metal lift-off procedure was used to dissolve unexposed resist resulting in the lift-off of the unwanted metal layer surrounding the thin film strip features. The metal lift off procedure consisted of immersing the Si chip in acetone for $\sim$5 min. Finally each sample was rinsed in acetone followed by isopropyl alcohol and blown dry using N$_2$ gas to remove any remaining debris from the Si chip samples.

Ultraviolet, Pulsed Laser Irradiation. A Lambda Physik LPX-305i, KrF excimer laser (248 nm wavelength), with a full width at half-maximum pulse duration of $\sim$18 ns was used to irradiate the Ni thin film strips. The beam emerging from the lasing cavity was directed to an optical bench that contained an aperture for trimming the incoming beam to its most uniform, central portions and to define an object for focusing the beam through a fused-silica lens onto the samples. All laser treatments reported in this paper were conducted in air. A photon fluence range of 380$-$420 mJ/cm^2 was explored to induce liquid phase, thin film dewetting, and the number of pulses investigated ranged from 1 up to 20 laser pulses. This laser fluence was adequate to melt the Ni thin films as characterized by scanning electron microscopy.

Thin Film Strip Dimensions. Thin film strips were patterned with strip widths (w, Figure 1a) ranging from 400 nm to 2.05 μm in order to yield rivulet radii (R$_o$, Figure 1b) according to equation 1. For example, rivulet radii of 130 $\pm$ 18nm (w = 1.4 μm) and 165 $\pm$ 9nm (w = 2.05 μm) were measured following PLiD demonstrating both (1) the validity of eq 1 for our retraction scheme and (2) minimal loss of Ni via evaporation or diffusion into the substrate.

Energy Dispersive Spectroscopy. Energy dispersive spectroscopy (EDS) measurements were collected using an EDAX Apollo XL instrument, attached to a FEI Nova 600 dual ion/ electron beam microscope, which was equipped with a 30 mm^2 active detection area. An electron accelerating voltage of 10 keV was used to excite X-ray emission in an image capture area of 256 $\times$ 200 pixels in order to create a Ni and Si composition map over a region of interest containing Ni rivulets, as well as Ni nanoparticles, in order to determine the Ni purity following PLiD. Negligible intermixing between the Si substrate and dewetted Ni was found which led to the conclusion that the rivulets and nanoparticles were Ni. The pixel size during X-ray acquisition was 50 nm. An accumulation number of 64 images were averaged to yield the final image EDS composition map. The dwell time per pixel per scan was 50 μs. Nickel is represented as red in the two-dimensional EDS derived composition maps and silicon is represented in the green channel (Figure 1g).

■ ASSOCIATED CONTENT

ⓢ Supporting Information. Details related to the experimental methods, simulation methods, and control experiments

used to support this research work. The material is available free of charge via the Internet at http://pubs.acs.org.

■ REFERENCES

(1) Favazza, C.; Kalyanaraman, R.; Sureshkumar, R. Robust nanopatterning by laser-induced dewetting of metal nanofilms. *Nanotechnology* **2006**, *17*, 4229–4234.

(2) Becker, J.; et al. Complex dewetting scenarios captured by thin-film models. *Nat. Mater.* **2003**, *2*, 59–63.

(3) Seemann, R.; Herminghaus, S.; Jacobs, K. Dewetting patterns and molecular forces: A reconciliation. *Phys. Rev. Lett.* **2001**, *86*, 5534–5537.

(4) Koc, A. 3-D analysis of temperature distribution in the material during pulsed laser and material interaction. *Heat Mass Transfer* **2004**, *40*, 697–706.

(5) Rack, P. D.; Guan, Y.; Fowlkes, J. D.; Melechko, A. V.; Simpson, M. L. Pulsed laser dewetting of patterned thin metal films: A means of directed assembly. *Appl. Phys. Lett.* **2008**, *92*, 223108.

(6) Favazza, C.; Trice, J.; Krishna, H.; Kalyanaraman, R. Laser-induced patterning of Co nanostructures under ambient conditions. *Mater. Res. Soc. Symp. Proc.* **2006**, *890*, 153–158.

(7) Fowlkes, J. D.; Wu, Y. Y.; Rack, P. D. Directed Assembly of Bimetallic Nanoparticles by Pulsed-Laser-Induced Dewetting: A Unique Time and Length Scale Regime. *ACS Appl. Mater. Interfaces* **2010**, *2*, 2153–2161.

(8) Xia, Q. F.; Chou, S. Y. The fabrication of periodic metal nanodot arrays through pulsed laser melting induced fragmentation of metal nanogratings. *Nanotechnology* **2009**, *20*, 285310.

(9) Diez, J. A.; Gonzalez, A. G.; Kondic, L. On the breakup of fluid rivulets. *Phys. Fluids* **2009**, *21*, 082105.

(10) Chou, S. Y.; Xia, Q. F. Improved nanofabrication through guided transient liquefaction. *Nat. Nanotechnol.* **2008**, *3*, 369–369.

(11) Rayleigh, L. On the instability of a cylinder of viscous liquid under capillary force. *Philos. Mag.* **1892**, *34*, 145–154.

(12) Brochard-Wyart, F.; Redon, C. Dynamics of Liquid Rim Instabilities. *Langmuir* **1992**, *8*, 2324–2329.

(13) Taylor, G. The Dynamics of Thin Sheets of Fluid 0.2. Waves on Fluid Sheets. *Proc. R. Soc. London, Ser. A* **1959**, *253*, 296–312.

(14) Sekimoto, K.; Oguma, R.; Kawasaki, K. Morphological Stability Analysis of Partial Wetting. *Ann. Phys. (San Diego, CA, U.S.)* **1987**, *176*, 359–392.

(15) Eggers, J.; Villermaux, E. Physics of liquid jets. *Rep. Prog. Phys.* **2008**, *71*, 036601.

(16) Plateau, J. A. F. *Acad. Sci. Brux. Mem.* **1843**, *16*, 3.

(17) Lian, J.; Wang, L. M.; Sun, X. C.; Yu, Q. K.; Ewing, R. C. Patterning metallic nanostructures by ion-beam-induced dewetting and Rayleigh instability. *Nano Lett.* **2006**, *6*, 1047–1052.

(18) Kondic, L.; Diez, J. A.; Rack, P. D.; Guan, Y. F.; Fowlkes, J. D. Nanoparticle assembly via the dewetting of patterned thin metal lines: Understanding the instability mechanisms. *Phys. Rev. E* **2009**, *79*, 026302.

(19) Van Orden, D.; Fainman, Y.; Lomakin, V. Optical waves on nanoparticle chains coupled with surfaces. *Opt. Lett.* **2009**, *34*, 422–424.

(20) Bader, S. D. Colloquium: Opportunities in nanomagnetism. *Rev. Mod. Phys.* **2006**, *78*, 1–15.

(21) Chien, C. L.; Zhu, F. Q.; Zhu, J. G. Patterned nanomagnets. *Phys. Today* **2007**, *60*, 40–45.

(22) Stipe, B. C. et al. Magnetic recording at 1.5 Pb m^{-2} using an integrated plasmonic antenna. *Nat. Photonics* **2010**, *4*, 484–488.

(23) Rahman, M. T.; Shams, N. N.; Lai, C. H. Nonlithographic fabrication of 25 nm magnetic nanodot arrays with perpendicular anisotropy over a large area. *J. Appl. Phys.* **2009**, *105*, 07C112.

(24) Wu, Y.; Fowlkes, J. D.; Rack, P. D.; Diez, J. A.; Kondic, L. On the Breakup of Patterned Nanoscale Copper Rings into Droplets via Pulsed-Laser-Induced Dewetting: Competing Liquid-Phase Instability and Transport Mechanisms. *Langmuir* **2010**, *26*, 11972–11979.

(25) Vrij, A.; Overbeek, J. T. Rupture of Thin Liquid Films Due to Spontaneous Fluctuations in Thickness. *J. Am. Chem. Soc.* **1968**, *90*, 3074–3078.

(26) Krishna, H.; Favazza, C.; Gangopadhyay, A. K.; Kalyanaraman, R. Functional nanostructures through nanosecond laser dewetting of thin metal films. *JOM* **2008**, *60*, 37–42.

(27) McCallum, M. S.; Voorhees, P. W.; Miksis, M. J.; Davis, S. H.; Wong, H. Capillary instabilities in solid thin films: Lines. *J. Appl. Phys.* **1996**, *79*, 7604–7611.

(28) Giermann, A. L.; Thompson, C. V. Solid-state dewetting for ordered arrays of crystallographically oriented metal particles. *Appl. Phys. Lett.* **2005**, *86*, 121903.

(29) Kim, D.; Giermann, A. L.; Thompson, C. V. Solid-state dewetting of patterned thin films. *Appl. Phys. Lett.* **2009**, *95*, 121903.

(30) Luber, E. J.; Olsen, B. C.; Ophus, C.; Mitlin, D. Solid-state dewetting mechanisms of ultrathin Ni films revealed by combining in situ time resolved differential reflectometry monitoring and atomic force microscopy. *Phys. Rev. B* **2010**, *82*, 085407.

(31) Zhang, L.; Brunet, P.; Eggers, J.; Deegan, R. D. *Phys. Fluids* **2010**, *22*, 122105.

(32) Snoeijer, J. H.; Le Grand-Piteira, N.; Limat, L.; Stone, H. A.; Eggers, J. Cornered drops and rivulets. *Phys. Fluids* **2007**, *19*, 042104.